Zinc Stable Isotope Fractionation Mechanisms during Adsorption on and Substitution in Iron (Hydr)oxides

Xinran Yan[1], Wei Li[2], Chuanwei Zhu[3], Caroline L. Peacock[4], Yizhang Liu[3], Hui Li[5], Jing Zhang[6], Mei Hong[7], Fan Liu[1], Hui Yin[1,*]

[1]Key Laboratory of Arable Land Conservation (Middle and Lower Reaches of Yangtse River), Ministry of Agriculture and Rural affairs, College of Resources and Environment, Huazhong Agricultural University, Wuhan 430070, China

[2]Key Laboratory of Surficial Geochemistry, Ministry of Education, School of Earth Sciences and Engineering, Nanjing University, Nanjing 210023, China

[3]State Key Laboratory of Ore Deposit Geochemistry, Institute of Geochemistry, Chinese Academy of Sciences, Guiyang 550002, China

[4]School of Earth and Environment, University of Leeds, Leeds, LS2 9JT, UK

[5]Department of Crop and Soil Sciences, North Carolina State University, Raleigh, North Carolina 27695, USA

[6]Beijing Synchrotron Radiation Facility, Institute of High Energy Physics, Chinese Academy of Sciences, Beijing 100039, China

[7]College of Grassland, Resources and Environment, Inner Mongolia Agricultural University, Hohhot 010018, China

Corresponding Authors:

Tel.: +86 27 87280271. Fax: +86 27 87288618.

Email: yinhui666@mail.hzau.edu.cn.

ABSTRACT: Zn isotope fingerprint is widely used as a proxy of various environmental geochemical processes, so it is crucial to determine which are the mechanisms responsible for isotopic fractionation. Iron (Fe) (hydr)oxides greatly control the cycling and fate and thus isotope fractionation factors of Zn in terrestrial environments. Here, Zn isotope fractionation and related mechanisms during adsorption on and substitution in three FeOOH polymorphs are explored. Results demonstrate that heavy Zn isotopes are preferentially enriched onto solids, with almost similar isotopic offsets ($\Delta^{66/64}Zn_{solid\text{-}solution}$=0.25-0.36‰) for goethite, lepidocrocite and feroxyhyte. This is consistent with the same average Zn-O bond lengths for adsorbed Zn on these solids as revealed by Zn K-edge X-ray absorption fine structure spectroscopy. In contrast, at an initial Zn/Fe molar ratio of 0.02, incorporation of Zn into goethite and lepidocrocite by substituting for lattice Fe preferentially sequesters light Zn isotopes with $\Delta^{66/64}Zn_{substituted\text{-}stock\ solution}$ of −1.52±0.09‰ and −1.18±0.15‰, while Zn-substituted feroxyhyte (0.06±0.11‰) indicates almost no isotope fractionation. This is closely related to the different crystal nucleation and growth rates during the Zn-doped FeOOH formation processes. These results provide direct experimental evidence of incorporation of isotopically light Zn into Fe (hydr)oxides, and improve our understanding of Zn isotope fractionation mechanisms during mineral-solution interface processes.

KEYWORDS: metal (hydr)oxides, metal isotope fractionation, interface reactions, isomorphous substitution, adsorption, X-ray absorption fine structure spectroscopy

SYNOPSIS

Structures, crystal nucleation and growth rates of FeOOH polymorphs affect Zn isotope fractionation during adsorption and substitution.

TOC Art

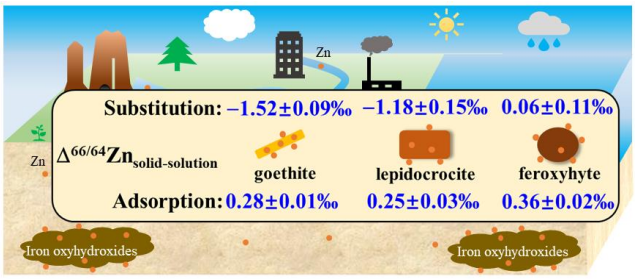
Zn
Substitution: −1.52±0.09‰ −1.18±0.15‰ 0.06±0.11‰
Zn
Δ66/64Znsolid-solution
goethite
lepidocrocite
feroxyhyte
Adsorption: 0.28±0.01‰ 0.25±0.03‰ 0.36±0.02‰
Iron oxyhydroxides
Iron oxyhydroxides

1. INTRODUCTION

Though an essential micronutrient at low concentrations, zinc (Zn) is toxic at high concentrations.[1] In terrestrial environments, high concentrations of Zn mainly result from intensive anthropogenic activities, including those associated with mining, smelting, chemical industries, agriculture, scrap disposal, combustion of domestic wastes and processing of domestic waste waters as well as runoff from urban surfaces, but Zn also originates from natural sources, such as natural weathering and hydrothermal emissions.[2] As a result of these anthropogenic activities and natural processes, Zn-containing particles are released and subsequently weathered, and the release of dissolved Zn to soils as a result of weathering processes is probably the greatest source of Zn in the environment.[3] Once released and in order to better understand and predict Zn behavior, recent research is increasingly focused on the isotopic signatures associated with Zn biogeochemical cycling because these can fingerprint the different Zn sources, processes and pathways that release Zn and control Zn mobility and fates.[4-8] The isotopic features of different Zn sources may be blurred however, by the biogeochemical processes and pathways that control its behavior, creating a "black box" of isotope signals that are extremely difficult to disentangle.[12] In particular once Zn is released into the environment, Zn isotopes might be fractionated by a series of solid-solution interfacial reactions, such as adsorption, substitution and coprecipitation with minerals,[9-13] and mineral dissolution[4, 14-16]. It is thus critical to investigate Zn isotope fractionation during these interfacial processes in order to use Zn isotopic signals to trace and track Zn in contaminated and natural systems.

In surficial environments, iron (Fe) (hydr)oxides play an important role in mediating the geochemical behavior and fate of metals in soils, sediments and waters through adsorption and isomorphous substitution. While metal isotope fractionation during adsorption onto mineral surfaces is well-studied,[9, 10, 18-21] few studies have been conducted on fractionation during incorporation into Fe (hydr)oxide structures[17]. During adsorption processes, mineral crystalline structure, distribution of charge within the crystal lattices, presence of organic or mineral coatings and solution chemistry may govern metal binding mechanisms and thus metal isotope fractionation direction and

magnitude.[19, 22] Previous work has reported that heavy Zn isotopes are preferentially adsorbed onto Fe (hydr)oxides with the fractionation magnitude for goethite much smaller than that for ferrihydrite.[19] Other studies however, observe negative Zn isotope fractionations induced by adsorption onto Fe (hydr)oxides at acidic conditions.[18, 23, 24] During Zn adsorption onto quartz and amorphous silica, the fractionation magnitude for the former is much smaller than that for the latter, probably due to the different surface structural characteristics (e.g., structural disorder).[25] These results suggest that there may be different Zn isotope fractionation during adsorption onto different FeOOH polymorphs, which yet remains to be investigated.

Metal isotope fractionation induced by incorporation into the mineral structures involves much complex mechanisms. This process is generally interpreted from a kinetic fractionation effect, in which light isotopes are preferentially incorporated into the mineral structure owing to faster diffusion rates than heavy isotopes.[26-28] Isotope fractionation can also be caused by preferential attachment of one specific metal species onto the host mineral primary nuclei growth sites after fast aqueous isotopic exchange.[29] Crystal nucleation and growth mechanisms can also be particularly important. Isotope fractionation of Cd during incorporation into goethite for example, is probably related to the ferrihydrite dissolution-goethite recrystallization mechanism.[17] Last but not least, host mineral crystallization rate may affect the fractionation magnitude.[26, 28, 30] Despite the role that incorporation into Fe (hydr)oxides plays in controlling Zn mobility and fate, the isotope fractionation of Zn during this process and the mechanism(s) responsible for governing Zn isotope behavior are unknown.

Here we aim to determine Zn isotope fractionation mechanisms during incorporation and adsorption with FeOOH polymorphs, including goethite (Goe), lepidocrocite (Lep) and feroxyhyte (Fero). The different structures of these FeOOH polymorphs may mean different crystal nucleation and growth mechanisms, metal uptake amounts[31] and metal binding mechanisms[32]. It is therefore possible that incorporation and adsorption of Zn with these FeOOH polymorphs may induce different isotope fractionations. Zn K-edge X-ray absorption fine structure spectroscopy (XAFS) and spherical aberration-corrected scanning transmission

electron microscopy are used to determine Zn binding mechanisms in substituted and adsorbed Fe (hydr)oxide minerals. The mineral crystal nucleation and growth mechanisms, crystallization rates and Zn binding mechanisms are then coupled to the Zn isotope fractionation during incorporation in and adsorption on these FeOOH polymorph minerals.

2. MATERIALS AND METHODS

All reagents were used as received without further purification and detailed information is presented in Text S1. The $ZnCl_2$ (≥98.0%, Sinopharm Chemical Reagent Co., Ltd, China) used in Zn-substituted FeOOH polymorph synthesis had a Zn isotope composition ($\delta^{66/64}$Zn) of –0.21±0.05‰, while that of the 1000 mg·L^{-1} $Zn(NO_3)_2$ bulk solution (Guobiao Testing & Certification Co., Ltd, China) used in Zn adsorption experiments was –2.40±0.05‰.

2.1 Preparation of Zn Substituted FeOOH Polymorphs

Zinc-substituted FeOOH polymorphs with an initial Zn/Fe molar ratio of 0.02 were synthesized according to our previous study.[31] For Zn-substituted goethite (Goe), firstly 90 mL of 5 M NaOH solution was added to 50 mL of 1 M $FeCl_3·6H_2O$ and 20 mM $ZnCl_2$ mixture in an acid-cleaned 1 L Teflon bottle. Subsequently, the obtained suspension was diluted to 1 L with ultrapure water (18.2 MΩ·cm) under stirring until the pH was adjusted to >13, and aged for 60 h at 70 °C. For Zn-substituted lepidocrocite (Lep), 16 g $FeCl_2·4H_2O$, 22.4 g $(CH_2)_6N_4$, 5.6 g $NaNO_2$ and 0.22 g $ZnCl_2$ solids were added to 560 mL ultra-pure water in an acid-cleaned 1 L Teflon bottle (the pH of the suspension was ~6.2) and then put in water bath kettle under stirring at 60 °C for 3 h. For Zn-substituted feroxyhyte (Fero), 5 M NaOH solution was added to 300 mL of 0.1 M $FeCl_2·4H_2O$ and 2 mM $ZnCl_2$ mixture to adjust the suspension pH to 8 under vigorously stirring in an acid-cleaned 1 L Teflon bottle, then 30% H_2O_2 was added to the solution. The obtained green suspension gradually transformed into a reddish brown precipitate and no further bubbles formed after ~1 h.

At the end of each synthesis, 50 mL of suspension was withdrawn under vigorously stirring, and the solid and solution were separated by centrifugation. The solution was kept for further analysis and labeled as “supernatant” in order to

differentiate it from that obtained during Zn adsorption experiments. The obtained solids (named as Zn2Goe, Zn2Lep and Zn2Fero, respectively) were treated with 50 mL 2 M HNO_3 solution for 0.5 h to remove adsorbed Zn species on the mineral surfaces (This part of Zn was labelled as "Adsorbed").[33] The remaining solids were named as Zn2Goe_n, Zn2Lep_n and Zn2Fero_n.

In order to monitor the crystal formation processes, independent synthetic experiments were conducted. 25 mL suspension was withdrawn at predetermined time intervals after heating of the initial reactant mixtures during the Zn-substituted Goe and Lep synthesis or upon the addition of H_2O_2 into the initial reactants during Zn-substituted Fero synthesis. The final pH values of the suspensions were 12.65±0.05, 5.32±0.05 and 2.22±0.05, respectively. The suspensions were immediately centrifuged, and as-obtained solids were thoroughly washed and then freeze dried for further use.

2.2 Sample Characterization

Pure Goe, Lep and Fero samples were synthesized as described above without the addition of Zn. The purity of the obtained solid samples was confirmed by powder X-ray diffraction (XRD) analysis (Figure S1). Quantitative phase analysis or Rietveld structure refinement of the intermediate solids during the synthesis of Zn-doped FeOOH polymorphs was conducted using TOPAS software version 4.2 (Bruker-AXS).[17] The specific surface areas of Goe, Lep and Fero were determined to be 46, 168 and 116 $m^2 \cdot g^{-1}$ by multipoint BET modelling of the N_2 physical adsorption data, while the points of zero charge (PZCs) of these samples were measured to be ~9.7, ~8.5 and ~9.4 respectively by adopting a Zeta potential method[17] (Figure S2). The sample morphologies were probed by electron microscopy (JEM-2010 HT, Japan) (Figure S3). The atomic images of Zn2Goe_n and Zn2Lep_n were obtained on a JEM-NEOARM spherical aberration-corrected scanning transmission electron microscopy at 200 kV (JEOL, Japan). Energy dispersive X-ray spectroscope (EDS) quantitative analysis of single crystals for each mineral was also conducted.

The Fe and Zn concentrations in the solutions and solids were measured by flame atomic adsorption spectrometry (FAAS, Agilent Technologies 200 series AA) or inductively coupled plasma-optical emission spectrometry (ICP-OES, Agilent 5110).

The limit of detection for Zn by FAAS is 4.76 $\mu g \cdot L^{-1}$ with an uncertainty of 0.4%, while for ICP-OES is 9 $\mu g \cdot L^{-1}$ with an uncertainty of 2.0%.

2.3 Adsorption Experiments

The minerals were hydrated in 0.05 M KNO_3 solution for 24 h before Zn addition. For kinetic adsorption experiments, 91.7 or 152.9 μM Zn was reacted with 1 $g \cdot L^{-1}$ Goe, or 0.5 $g \cdot L^{-1}$ Lep and Fero at pH 7±0.05 for 48 h, during which suspension aliquots were withdrawn at predetermined intervals. Adsorption edge experiments were conducted between pH 4.0-8.0. Adsorption isotherms were conducted with Zn initial concentrations of 0-305.8 μM for Goe or 0-611.5 μM for Lep and Fero at pH 7±0.05. The initial Zn concentrations were designed to obtain similar Zn coverages on these solids and to prevent Zn precipitation. The suspension pH was maintained by the addition of 1 M HNO_3 or KOH solution. All adsorption experiments were conducted in Teflon tubes. A reaction time of 24 h was adopted by assuming that both adsorption and isotope fractionation equilibrium are approached according to literature.[19, 34]

At the end of experiments, solids and supernatants were separated through 0.2 μm cellulose membranes. To remove dissolved Zn the solids were immediately washed with background electrolyte and sequentially ultrapure water, the pHs of which were adjusted to be consistent with the adsorption experiments.[19] The washed solids were collected with membranes, sealed with Kapton tape and then stored at 4 °C within 24 h for further Zn K-edge XAFS analysis. The Zn concentrations in the supernatants and solids after digestion were measured by FAAS. The obtained Zn-loaded solids were labeled as ZnmGoe_pHn, ZnmLep_pHn and ZnmFero_pHn, in which m is the initial Zn concentration in $mg \cdot L^{-1}$ and n is the reaction pH. Replicated experiments were carried out 2-3 times to ensure reproducibility.

A Zn adsorbed ferrihydrite (Fh) standard, Zn20Fh_pH7.5, was also prepared by reacting 0.31 mM Zn with 0.5 $g \cdot L^{-1}$ Fh (synthesized according to a previous study)[17] for 24 h at pH 7±0.05 in 0.05 M KNO_3 solution.

2.4 Purification and Measurement of Zn Isotopes by MC-ICP-MS

Zinc-containing solids were digested using 12 M HCl and 15 M HNO_3 solutions until dry and then redissolved in 2 M HCl solution. About 3 μg Zn was weighted for

Zn purification. After drying, 2 mL of 2 M HCl was added, and the solution was transferred into a 15 mL polypropylene centrifuge tube. Samples were then purified on columns containing 3 mL of pre-cleaned 100–200 mesh AG MP-1M (Bio-Rad, USA) anion-exchange resin.[35, 36] After the adsorption of metals onto the column, 30 mL of 2 M HCl and 12 mL of 0.3 M HCl were passed through the columns, respectively. Zn was eluted using 12 mL of 0.012 M HCl. The solution was evaporated to dryness at 110 °C and dissolved in 3 mL of 1% HNO_3. Additionally, 0.5 mL of the final solution was used for Zn measurement to monitor the recovery, and the residue was used for Zn isotope analysis. Satisfactory recoveries were obtained for the unprocessed and processed samples (> 98%).

Zinc isotope ratios were measured using a Thermo Scientific Neptune plus MC-ICP-MS at the State Key Laboratory of Crust–Mantle Evolution and Mineralization at Nanjing University. Instrumental mass bias was corrected using a coupled method of sample-standard bracketing (SSB) and Cu doping. More details are provided in Text S2. Sample Zn isotope ratios were reported in standard delta notation in per mil units relative to IRMM 3702 Zn solution according to Eq. 1:

$$\boldsymbol{\delta}^{66/64}\mathrm{Zn}=\left[\frac{(^{66}\mathrm{Zn}/^{64}\mathrm{Zn})_{\mathrm{sample}}}{(^{66}\mathrm{Zn}/^{64}\mathrm{Zn})_{\mathrm{std}}}-1\right]\times 1000 \quad (1)$$

Since a mass dependent fractionation law applies to all samples (Figure S4), only $\delta^{66/64}$Zn was reported. CAGS-1 and the new AA-ETH Zn isotope standard solutions were used as internal laboratory secondary reference materials, and the $\delta^{66/64}\mathrm{Zn}_{\mathrm{IRMM\ 3702}}$ values were −0.85±0.05‰ (n=6) and −0.01±0.05‰ (n=6) respectively, agreeing well with previously reported values.[35, 37] An in-house sulphide standard (BCR-2) was used to monitor potential Zn isotope fractionation during purification, and the analyses of BCR-2 yielded $\delta^{66/64}\mathrm{Zn}_{\mathrm{JMC\text{-}Lyon}}$ of 0.28±0.02‰ (n=2), consistent with reported values.[38] The long-term reproducibility of 0.05‰ was used for data measured with 2SD value of < 0.05‰. The Zn isotope fractionation ($\Delta^{66/64}\mathrm{Zn}_{\mathrm{solid\text{-}solution}}$) between solid and aqueous phases is defined as Eq. 2:

$$\Delta^{66/64}\mathrm{Zn}_{\mathrm{solid\text{-}solution}}=\delta^{66/64}\mathrm{Zn}_{\mathrm{solid}}-\delta^{66/64}\mathrm{Zn}_{\mathrm{solution}} \quad (2)$$

2.5 Zn K-edge XAFS Data Collection and Analysis

Zinc K-edge XAFS spectra for Zn-containing samples along with aqueous $Zn(NO_3)_2$ were collected on beamline 1W2B at BSRF at room temperature with a pair of Si(111) monochromators in fluorescence or transmission mode. The Zn metal foil (E_0 = 9659 eV) was used for energy calibration. The data processing and analysis were performed using the IFEFFIT software.[39] The parameters used for background removal were: E_0 = 9667 eV, k-weight = 2 and R_{bkg} = 1.1. Structural parameters (R, CN, and σ^2) were obtained by fitting the experimental k^2-weighted data to the standard equation.[40] An amplitude reduction factor (S_0^2) of 0.85 was used.[20]

3. RESULTS AND DISCUSSION

3.1Zn Isotope Fractionation during Adsorption on FeOOH Polymorphs

Similar Zn adsorption kinetics, pH adsorption edges and adsorption isotherms are observed for these FeOOH polymorphs (Figure S5 and Table S1). The maximum Zn adsorption densities on Goe, Lep and Fero obtained by Langmuir fitting are 2.47, 2.62 and 4.12 μmol·m^{-2}, respectively (Table S2).

Analysis of the isotopic compositions of the solutions and solids shows that heavy Zn isotopes are preferentially enriched on the mineral surfaces. As the reaction pH raises from 6 to 8, the proportion of Zn adsorbed (f) increases from 19.0 to 91.4% for Goe, from 18.1 to 92.7% for Lep and from 20.6 to 96.8% for Fero, while correspondingly, the $\delta^{66/64}Zn_{solution}$ value decreases from –2.42±0.05‰ to –2.62±0.05‰, from –2.50±0.05‰ to –2.77±0.05‰ and from –2.40±0.08‰ to –2.61±0.05‰ (Table S3). When the isotopic compositions are plotted as a function of f (Figure 1), it is clear that experimental $\delta^{66/64}Zn$ values in the solutions and solids linearly decrease as f increases. The data are fitted with both an equilibrium (Eq. 3) and Rayleigh model (Eq. 4):

$$\delta^{66/64}Zn_{solution} = \frac{\delta^{66/64}Zn_{stock\ solution} - 1000 \cdot f(\alpha_{solid\text{-}solution} - 1)}{1 + f(\alpha_{solid\text{-}solution} - 1)} \quad (3)$$

$$\delta^{66/64}Zn_{solution} = (1000 + \delta^{66/64}Zn_{stock\ solution}) \cdot (1 - f)^{(\alpha_{solid\text{-}solution}-1)} - 1000 \quad (4)$$

Where $\alpha_{solid\text{-}solution}$ represents the estimated isotope fractionation factor between adsorbed and aqueous Zn, and $\delta^{66/64}Zn_{stock\ solution}$ denotes the estimated value for stock solution. The equilibrium model applies to systems in which forward and backward reactions occur at similar rates, while the Rayleigh model applies to homogeneous reactant pools where light isotopes are continuously and preferentially removed.[41]

The fits generated using the equilibrium model agree much better with the experimental data than those using the Rayleigh model. This demonstrates that Zn isotope fractionation during adsorption onto the FeOOH polymorphs results from an equilibrium fractionation mechanism. The derived fractionation factors ($\alpha_{solid\text{-}solution}$) are 1.00028± 0.00001, 1.00025±0.00003 and 1.00036±0.00002 for Goe, Lep and Fero, respectively. The isotope fractionation between adsorbed and dissolved Zn can be calculated according to the isotope fractionation factor (Eq. 5):

$$\Delta^{66/64}Zn_{solid\text{-}solution} \cong 1000 \times \ln\boldsymbol{\alpha}_{solid\text{-}solution} \quad (5)$$

The $\Delta^{66/64}Zn_{solid\text{-}solution}$ are thus calculated to be 0.28±0.01‰, 0.25±0.03‰ and 0.36±0.02‰ for Goe, Lep and Fero, respectively. This suggests that Zn adsorption on these three FeOOH polymorphs induces a similar isotope fractionation.

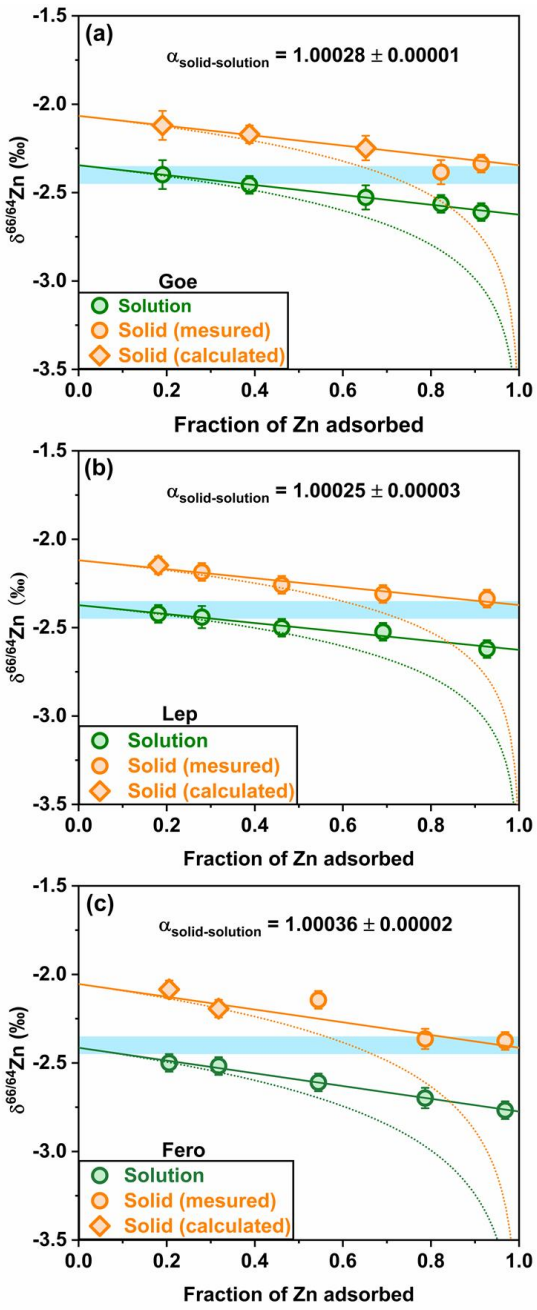

Figure 1. Zn isotopic compositions of solution and solid phases as a function of adsorbed Zn fraction (*f*) during adsorption onto Goe (a), Lep (b) and Fero (c). The lines and dashed curves represent the theoretical $\delta^{66/64}$Zn values calculated using the equilibrium model and the Rayleigh model, respectively. Several $\delta^{66/64}$Zn values of the solids (diamonds) were calculated according to the mass balance: $\delta^{66/64}Zn_{solid} = (\delta^{66/64}Zn_{stock\ solution} - \delta^{66/64}Zn_{solution} \times (1 - f))/f$. The $\delta^{66/64}$Zn of the bulk Zn solution used for adsorption experiments is –2.40±0.05‰.

3.2 Zinc Binding Environments in the Zn-containing Samples

Both Zn K-edge X-ray absorption near edge structure (XANES) and extended X-ray absorption fine structure (EXAFS) spectra were used to analyze the Zn binding mechanisms in typical Zn-containing samples. XANES spectra of all samples display broadening and/or splitting of the main edge at ~9672 eV (Figure 2A), due to the contribution of second Fe neighbors.[42] A well-defined peak at ~9688 eV is observed for aqueous $Zn(NO_3)_2$ and Zn-substituted samples Zn2Goe_n and Zn2Lep_n, suggesting that Zn is predominantly in octahedral (^{VI}Zn) geometry in the substituted samples and predominantly tetrahedral (^{IV}Zn) complexes in the adsorbed samples.[24, 42-44] Linear combination fitting of the adsorbed samples using Zn20Fh_pH7.5 and Zn2Goe_n as endmembers, in which exclusively ^{IV}Zn or ^{VI}Zn exists respectively,[19, 44-46] demonstrates that Zn adsorbed Fero samples contain only ^{IV}Zn, Zn adsorbed Lep samples contain 17-27% ^{VI}Zn, while Zn adsorbed Goe samples contain 31-40% ^{VI}Zn (Table S4). Previous studies have demonstrated that Zn is adsorbed on goethite as octahedral[19] but also tetrahedral complexes.[23, 47] The varying proportions of ^{IV}Zn and ^{VI}Zn may be related to the mineral characteristics and solution chemistry.

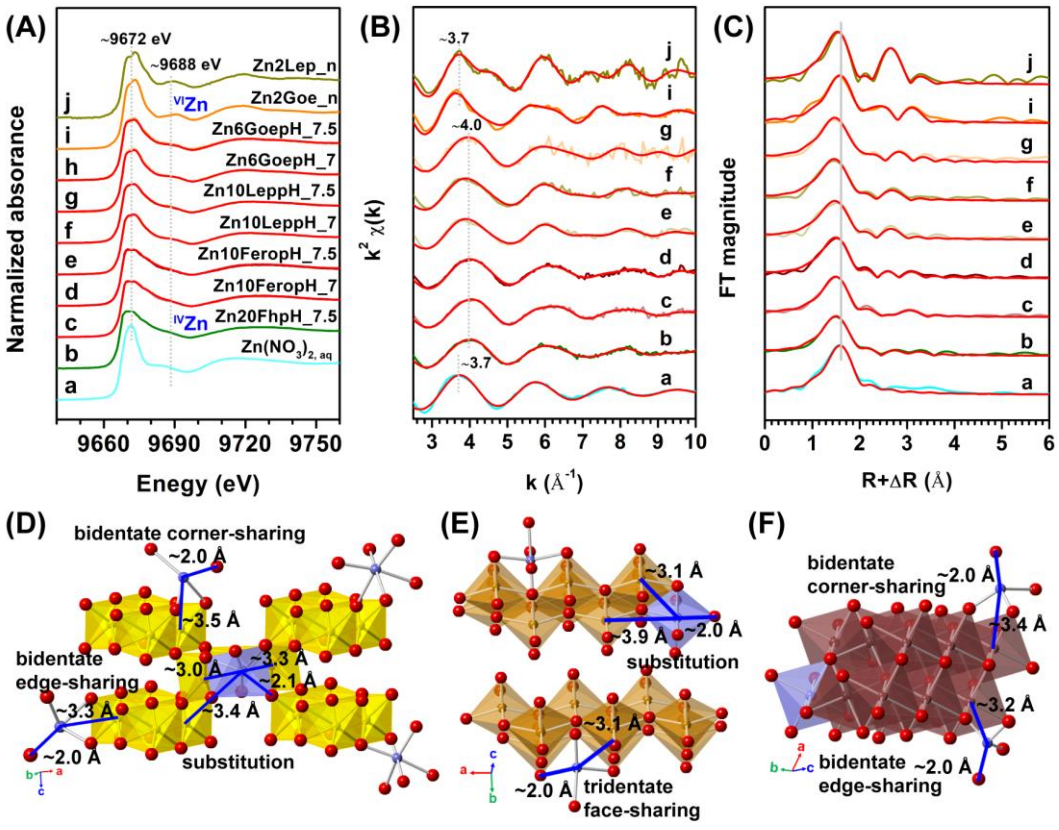

Figure 2. Zinc K-edge XANES (A), k^2-weighted EXAFS (B) and the corresponding

Fourier transformed spectra (FTs, C) of typical Zn adsorbed, substituted samples, and aqueous $Zn(NO_3)_2$ standard ($Zn(NO_3)_{2,aq}$), overlaid with the best fits. The experimental data are displayed as colored lines and the best fits are shown as red lines. The adsorbed samples were named as ZnmGoe_pHn, ZnmLep_pHn and ZnmFero_pHn, in which m is the initial Zn concentration in $mg \cdot L^{-1}$ and n is the reaction pH. The Zn substituted samples were labeled as ZnmGoe_n and ZnmLep_n, in which m is the initial Zn/Fe molar ratio. During linear combination fitting of the Zn K-edge XANES spectra for the Zn adsorbed samples, Zn adsorbed ferrihydrite sample (Zn20Fh_pH7.5) and Zn substituted goethite sample (Zn2Goe_n) were used as tetrahedral (^{IV}Zn) and octahedral (^{VI}Zn) endmembers. A schema representing the local environments of Zn adsorbed onto and incorporated into goethite (D), lepidocrocite (E) and feroxyhyte (F).

In the k^2-weighted EXAFS spectra (Fig. 2B), there is a shift in the first oscillation of the Zn adsorbed samples to high k (~4.0 $Å^{-1}$) relative to that of the aqueous $Zn(NO_3)_2$ and Zn substituted samples (~3.7 $Å^{-1}$). This shift indicates a change of Zn-O first shell coordination from octahedral to tetrahedral,[48] further confirming the XANES analysis. In the Fourier transformed spectra (Fig. 2C), the obvious peaks beyond the first Zn-O shell indicate the formation of Zn inner-sphere complexes on the mineral surfaces or incorporation into the lattices. Shell-by-shell EXAFS fitting (Table S4) shows an average Zn-O distance of 2.07±0.01 Å for aqueous $Zn(NO_3)_2$, and of 1.99±0.01 Å for ^{IV}Zn in Zn adsorbed ferrihydrite, which agree well with previous literature.[9, 19, 47, 49] Similar average Zn-O distances of 1.98-1.99 Å are observed for the Zn-adsorbed samples. These distances are closer to those for tetrahedral Zn. This is consistent with the linear combination fitting which shows that Zn adsorbed on Fero, Lep and Goe is predominantly tetrahedral but with an increasing amount of octahedral Zn, respectively (Table S4). Similar results were previously observed for Zn-O distances in hydrozincite (~2.00 Å),[9] Zn adsorbed on manganite (1.98-2.04 Å)[50] and on todorokite at pH6-8 (2.00-2.05 Å).[9] Two Zn-Fe distances of 3.12-3.25 Å and 3.35-3.49 Å are also observed for Zn adsorbed Fh, Fero and Goe. This indicates the formation of bidentate edge- and corner-sharing complexes on the mineral surfaces (Fig. 2D,F).[43, 19, 49] In contrast, only a Zn-Fe distance of 3.11-3.13 Å is detected for Zn adsorbed Lep, which can be assigned

to tridentate face-sharing complexes (Fig. 2E).[19] For Zn-substituted Goe, an average Zn-O distance of 2.07±0.01 Å and three Zn-Fe distances at 3.02±0.03 Å, 3.33±0.06 Å and 3.49±0.05 Å are observed. These distances correspond well to those observed for Zn substituted goethite.[51] For Zn-doped Lep, a Zn-O distance of 2.01±0.01 Å and two Zn-Fe distances of 3.11±0.02 Å and 3.90±0.08 Å support the incorporation of Zn into the mineral lattices according to the mineral crystal structure.

3.3 Isotope Fractionation Mechanisms during Zn Adsorption on FeOOH Polymorphs

Our results clearly suggest that heavy Zn isotopes are preferentially partitioned onto the FeOOH mineral surfaces, which is in good agreement with previous studies.[10, 19, 20, 25] It was previously reported that heavy Zn isotopes are enriched on Fe, Si, Al and Mn (hydr)oxides surfaces during adsorption processes, owing to the formation of inner-sphere complexes with shorter Zn-O lengths compared to aqueous Zn.[19, 20, 25, 52, 53] Generally, heavier metal isotopes are preferentially concentrated in stiffer bonding environments, e.g. coordinated to highly covalent bonds, with lower coordination number and shorter bond lengths.[12, 41] The Zn K-edge XAFS analysis shows that Zn adsorbed onto Goe, Lep and Fero form inner-sphere complexes with Zn-O bond lengths ranging from 1.98-1.99 Å that are much shorter than that of octahedral Zn in solution (2.07±0.01 Å) (Table S4). These bond length differences are probably responsible for adsorption-induced enrichment of heavy Zn isotopes onto these FeOOH polymorphs. The fact that these Zn-O bond lengths are almost the same for the different FeOOH polymorphs (Table S4), also explains why we observe a similar $\Delta^{66/64}Zn_{solid\text{-}solution}$ of 0.25-0.36‰ for Goe, Lep and Fero. Though Zn K-edge XANES linear combination fitting shows that Zn is predominantly adsorbed as ^{IV}Zn on Fero, Lep and Goe but with increasing proportions of ^{VI}Zn in the latter two, EXAFS analysis, which fits the average bonding environment, gives essentially the same Zn-O distances. As such our results indicate that having only ^{IV}Zn (feroxyhyte) or a mixture of ^{IV}Zn-^{VI}Zn (goethite/lepidocrocite) does not significantly modify the recorded $\Delta^{66/64}Zn_{solid\text{-}solution}$ (difference < 0.1‰), which may be ascribed to the weaker effect of ^{VI}Zn than ^{IV}Zn on isotope fractionation magnitude during adsorption on Fe (hydr)oxides.[44]

It is noteworthy that although our study confirms the enrichment of heavy Zn isotopes during adsorption on Fe (hydr)oxides as revealed by some previous studies,[19] others observed negative $\Delta^{66/64}Zn_{solid\text{-}solution}$ during Zn adsorption on goethite at acid conditions (e.g., pH5.3-6.1)[18, 23, 24]. In contrast, positive $\Delta^{66/64}Zn_{solid\text{-}solution}$ is observed at higher pHs (6-8) here and in previous study[19]. We therefore hypothesize that pH and Zn solution speciation may play important roles in Zn isotope fractionation direction and magnitude.[18, 23] For example, relative to $Zn(H_2O)_6^{2+}$, $Zn(OH)(H_2O)_5^{+}$ and $Zn(OH)_2(H_2O)_4$, the proportions of which are increased at higher pH, enrich relatively heavy isotopes.[54] Speciation calculations in the current study however, show that aqueous $Zn(H_2O)_6^{2+}$ is the dominant species (~95%) with only limited $ZnNO_3(H_2O)_5^{+}$ (5%) over pH 4-8 (Figure S6). This suggests that Zn aqueous speciation contributes little to the Zn isotope fractionation during adsorption onto the FeOOH polymorphs in the present study. Thus it is possible that different isotope fractionation mechanisms dominate at low and high pH conditions during Zn adsorption onto goethite but confirmation of this requires further study.

3.4 Crystal Formation Processes of Zn-Substituted FeOOH Polymorphs

In order to better understand the Zn isotope fractionation during substitution into the FeOOH polymorph minerals, we first discuss the crystal growth processes. Powder XRD analysis of intermediate solids during Zn-substituted Goe synthesis shows the formation of goethite (ICSD 71870) via a ferrihydrite precursor (ICSD 158475) (Figure 3a,S7a).[17, 27, 55] Specifically, the diffraction peaks of goethite appear within 3 h, and then gradually increase with time and stay almost unchanged after 12 h. The ferrihydrite formed at 1 h has a coherent scattering domain (CSD) size of 2.6±0.4 nm (Figure 3a, Table S5). Quantitative phase analysis of the 3 h and 6 h solids shows 61±10% and 13±5% ferrihydrite, and the precursor is almost completely transformed to goethite at 12 h. The average CSD sizes of the goethite particles slightly increase from 27.0±0.2 nm at 12 h to 28.5±0.2 nm at 60 h. Owing to the high reaction pH (~12.7) and the reactivity of ferrihydrite/goethite towards metals, almost all the initial Zn is retained on the intermediate solids with constant Zn/Fe molar ratios of 1.8-1.9%.

Unlike the Zn-doped Goe system, there is probably no ferrihydrite precursor

417 during the Zn-doped Lep synthesis under the current experimental conditions (pH~5.3).
418 XRD patterns show the appearance of weak crystalline lepidocrocite (ICSD 108876)
419 after reaction for 1 min but without ferrihydrite (Figure 3b,S7b). This is consistent with
420 previous studies showing that lepidocrocite dominates upon Fe^{2+} oxidation at pH>5
421 while ferrihydrite dominates at pH < 5.[56] As the reaction progresses, a gradual increase
422 in the XRD peak intensity indicates increasing mineral crystallinity within 1 h. The
423 particle CSD size increases from 3.3±0.1 nm at 1 min to 7.6±0.1 nm at 1 h, and then
424 remains constant (Table S5). This may indicate that Lep is formed through a direct
425 nucleation and crystal growth mechanism. Concurrently, owing to the finite particle
426 size, at 1 min the solid has a Zn/Fe ratio of 1.9±0.0%. As the crystal grows and particle
427 size increases, some of the Zn may be released back into solution and at 30 min the
428 solid Zn/Fe ratio decreases to 1.3%. The solids from 1-3 h have Zn/Fe ratios of 1.5-
429 1.6%, probably owing to Zn re-adsorption onto the solid.
430 Similar to that of Zn-doped Lep formation, Fero crystal (ICSD 291515) is directly
431 formed by Fe^{2+} oxidation without ferrihydrite formation (Figure 3c,S7c).[56] The Fero
432 crystal nucleation and growth however, occur at much higher rates than those of Lep,
433 e.g., for Fero crystal nucleation and growth are almost complete in the first minute, as
434 evidenced by the almost unchanged XRD peak intensities and CSD sizes of the
435 intermediate solids (9.8-11.5 nm) as the reaction goes on (Table S5). The Zn/Fe molar
436 ratios in these intermediates slightly decrease from 1.0±0.0% in the 1 min solid to
437 0.8±0.0% in the 60 min solid, probably owing to the competition by protons for active
438 sites at a pH of ~2.2.

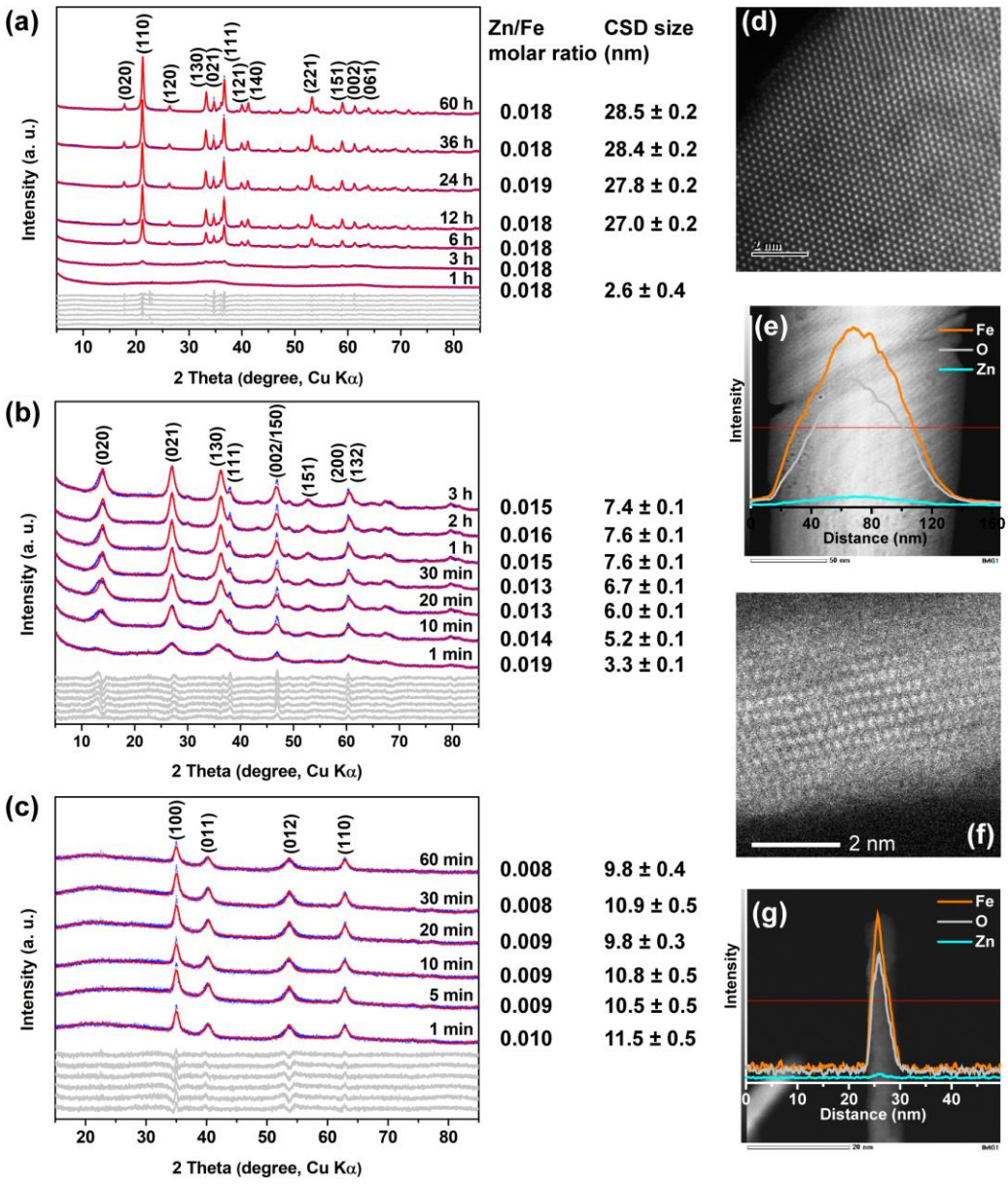

439

440 **Figure 3.** Powder XRD patterns, final Zn/Fe molar ratios and coherent scattering
441 domain (CSD) sizes of the reaction intermediates during the synthesis of Zn-substituted
442 goethite (a), lepidocrocite (b) and feroxyhyte (c). The XRD experimental patterns (blue
443 crosses) are overlaid with the best Rietveld structure refinement or quantitative phases
444 analysis results (red lines), based on the structure models of goethite (ICSD 71810),
445 ferrihydrite (ICSD 158475), lepidocrocite (ICSD 108876) and feroxyhyte (ICSD
446 291515). The difference patterns are shown as gray lines at the bottom. All experiments
447 were conducted at an initial Zn/Fe molar ratio of 0.02. Atomic resolution images and
448 EDS line scans of Zn-substituted goethite sample, Zn2Goe_n (d and f), and Zn-
449 substituted lepidocrocite sample, Zn2Lep_n (e and g).

The final molar ratios of Zn/Fe in Zn2Goe_n, Zn2Lep_n and Zn2Fero_n are 1.9±0.0%, 1.3±0.0% and 0.4±0.0%, respectively. Zn cations removed by HNO_3 treatment of Zn2Goe, Zn2Lep and Zn2Fero samples are probably those adsorbed on these mineral surfaces. This can be confirmed by several lines of evidence. Firstly, only 2.0%, 7.2% and 7.3% of the total Fe are removed from these samples (Figure S8). Secondly, powder XRD patterns of these samples before and after HNO_3 treatment are almost the same (Figure S9). Thus, the solids obtained after HNO_3 treatment are Zn-substituted minerals. Atomic images of Zn2Goe_n and Zn2Lep_n show the uniform distribution of Zn in the crystal lattices (Figure 3d,f). This is further confirmed by the EDS line scan of single crystals for each mineral that clearly shows the strong correlations between Fe, Zn and O (Figure 3e,g). Furthermore, the EDS analysis gives an average Zn/Fe molar ratio of 2.1±0.1% for Zn2Goe_n and 1.0±0.1% for Zn2Lep_n (Figure S10), which agree well with the wet chemical analysis results.

3.5 Zn Isotope Fractionation during Substitution for Fe in FeOOH Polymorphs

At the end of Zn2Goe synthesis, Zn isotope compositions in the supernatant ($\delta^{66/64}Zn_{supernatant}$) and in the solid ($\delta^{66/64}Zn_{Zn2Goe}$) are 1.27±0.05‰ and –0.15±0.07‰, respectively (Figure 4,S8). The latter is identical to the Zn stock solution (-0.21±0.05‰), due to the fact that almost all Zn is retained in Zn2Goe. After 2 M HNO_3 treatment, $\delta^{66/64}Zn$ for Zn incorporated into goethite ($\delta^{66/64}Zn_{Zn2Goe\_n}$) is –0.16±0.05‰, while $\delta^{66/64}Zn$ for Zn in HNO_3 solution ($\delta^{66/64}Zn_{Adsorbed}$) is –0.07±0.05‰ (Figure 4,S8). The $\delta^{66/64}Zn$ of Zn2Lep and the corresponding supernatant are –0.28±0.08‰ and 0.40±0.05‰, while $\delta^{66/64}Zn_{Zn2Lep\_n}$ and $\delta^{66/64}Zn_{Adsorbed}$ decrease to –0.45±0.05‰ and 0.12±0.08‰, respectively. In contrast, $\delta^{66/64}Zn$ of Zn2Fero and the corresponding supernatant are –0.09±0.05‰ and –0.25±0.05‰ respectively, while $\delta^{66/64}Zn_{Zn2Fero\_n}$ decreases to –0.24±0.05‰ and $\delta^{66/64}Zn_{Adsorbed}$ increases to 0.18±0.05‰.

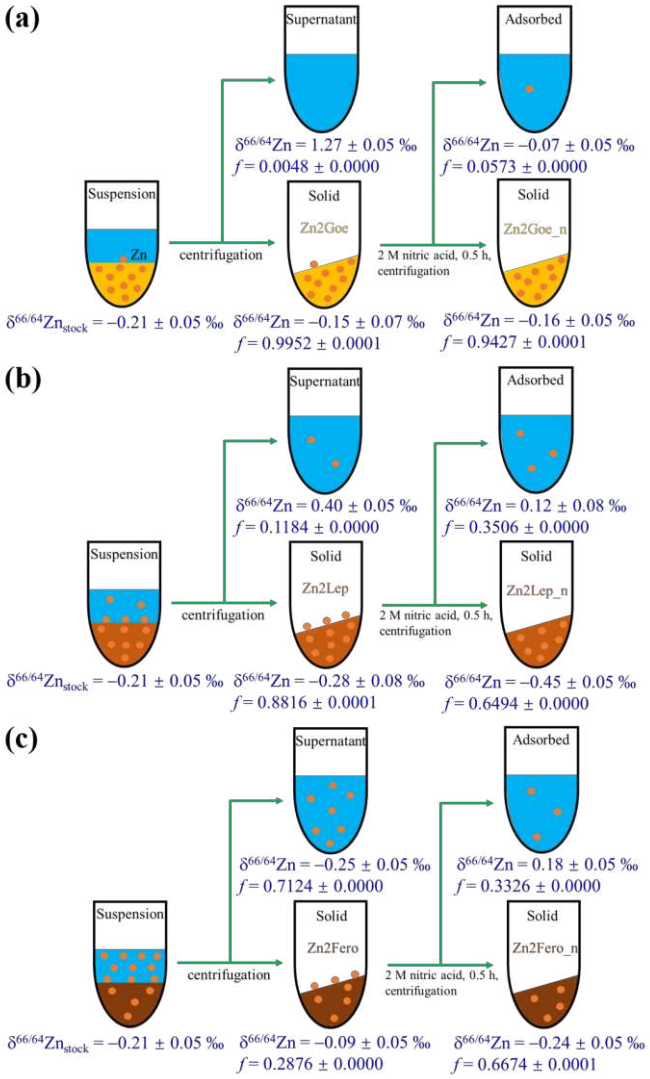

Figure 4. Schematic illustration of the experimental protocols for Zn isotope fractionation analysis during Zn substitution in (a) Goe, (b) Lep and (c) Fero. The Zn isotope composition and the fraction of Zn (*f*) at each step were presented. The $\delta^{66/64}$Zn of $ZnCl_2$ used for Zn-substituted FeOOH polymorphs synthesis is –0.21±0.05‰. It should be noted that the different *f* cannot be summed to obtain 100% and each step considers a new total population (100%), which is divided into two parts.

According to the isotope signals of different Zn pools during these processes, we can also calculate the Zn isotope compositions ($\delta^{66/64}Zn_{substituted}$) of the Zn-substituted FeOOH polymorph minerals (Eq. 6).

$$\delta^{66/64}Zn_{\text{stock solution}} = f_1 \times \delta^{66/64}Zn_{\text{supernatant}} + f_2 \times \delta^{66/64}Zn_{\text{adsorbed}} + f_3 \times \delta^{66/64}Zn_{\text{substituted}} \quad (6)$$

where f_1, f_2 and f_3 refer to the fractions of Zn in supernatant, adsorbed on the mineral surfaces, and incorporated into the crystal lattices, respectively. Based on Eq. 6, the $\delta^{66/64}Zn_{\text{substituted}}$ values are calculated to be –0.22±0.05‰, –0.46±0.09‰ and –0.14±0.10‰ for Zn2Goe_n, Zn2Lep_n and Zn2Fero_n respectively, which are consistent with the measured values. In these systems, adsorption and substitution processes both lead to the distribution of Zn between solution and solid and thus isotope fractionation.

If we assume that the two isotope fractionation factors involved here, for adsorption and incorporation, follow an equilibrium regime, the Zn isotope fractionation during incorporation into the lattices of these minerals ($\Delta^{66/64}Zn_{\text{substituted-stock solution}}$) can be calculated according to the isotope mass balance (Eq. 7):

$$\Delta^{66/64}Zn_{\text{solid-supernatant}} = f_2/(f_2 + f_3) \times \Delta^{66/64}Zn_{\text{adsorbed-supernatant}} + f_3/(f_2 + f_3) \times \Delta^{66/64}Zn_{\text{substituted-stock solution}} \quad (7)$$

where $\Delta^{66}Zn_{\text{solid-supernatant}}$ refers to Zn isotope fractionation between supernatant and solid at the end of the FeOOH formation, and equals -1.42±0.09‰, -0.68±0.09‰ and 0.16±0.07‰ for Zn2Geo, Zn2Lep and Zn2Fero, respectively. Thus, the $\Delta^{66/64}Zn_{\text{substituted-stock solution}}$ values are calculated to be –1.52±0.09‰, –1.18±0.15‰ and 0.06±0.11‰ for Zn2Goe_n, Zn2Lep_n and Zn2Fero_n respectively. These results clearly indicate that Zn substitution enriches light isotopes in goethite and lepidocrocite but almost no isotope fractionation occurs in feroxyhyte at the experimental conditions.

3.6 Zn Isotope Fractionation Mechanisms during Substitution for Fe in FeOOH Polymorphs

About >94% Zn is retained in the Zn2Goe_n solid by substituting for lattice Fe, and this results in a substantial negative isotope fractionation (–1.52±0.09‰) (Figures 4a,S8A). EXAFS analysis shows that Zn substitutes for lattice Fe in Zn2Geo_n with a Zn-O bond length the same as that (2.07±0.01 Å) for aqueous Zn. This suggests that

508 the enrichment of light Zn isotopes in Zn2Geo_n is not related to the Zn coordination
509 environment but rather is probably related to the goethite formation process. Goethite
510 generally forms from Fh dissolution-Goe recrystallization processes.[27, 55] In tandem
511 with the Fh formation, lighter Zn isotopes are preferentially incorporated in and/or
512 adsorbed onto the solid due to a kinetic effect, in which lighter isotopes diffuse faster
513 than heavier ones (e.g., within 1 h, Figure 3a). This results in the enrichment of heavy
514 Zn isotopes in the solution with $\delta^{66/64}Zn_{supernatant} > 1.27\pm0.05‰$. Subsequently, Fh
515 particles slowly dissolve, releasing into the solution soluble Fe as nucleus to form the
516 Goe and Zn species as suitable growth units (e.g., 1-12 h, Figure 3a). This process may
517 also be kinetically controlled, such that isotopically light Zn is released into the
518 surrounding solution. It was previous reported that in the early stages of proton- and
519 oxalate-promoted dissolution of finely powdered biotite granite, isotopically light Zn
520 was released following a kinetic isotope fractionation.[16] Further, the Zn released is
521 expected to be relatively isotopically light, because heavy Zn isotopes are preferentially
522 adsorbed on/incorporated in the ferrihydrite by adopting a tetrahedral geometry.[49]
523 Notwithstanding this, the released relatively light Zn isotopes are probably in
524 tetrahedral coordination.[19, 42, 49] After their release, a transformation from tetrahedral to
525 octahedral would occur and then the octahedral Zn is directly attached onto the goethite
526 growth unit. Alternatively, the released Zn tetrahedra can be immediately attached onto
527 the goethite growth unit and then transform to octahedra. Although all these kinetically
528 controlled isotope fractionation processes that are possibly involved during Zn
529 substitution in goethite can contribute to the enrichment of light Zn isotopes in the
530 goethite lattices, kinetic effects often occur in the first few hours of metal-mineral
531 interactions.[22] After this initial window, Zn adsorbed on the mineral surfaces and that
532 remaining in the supernatant exchange and reach adsorption/desorption equilibrium and
533 isotope fractionation equilibrium. Thus the 1.27±0.05‰ Zn isotope signal of the
534 supernatant at the end of Zn-doped goethite synthesis is possibly the result of a complex
535 series of kinetic and equilibrium processes. Further, the calculated large
536 $\Delta^{66/64}Zn_{substituted\text{-}stock\ solution}$ (−1.52±0.09‰) suggests that the isotope signal of Zn-
537 substituted goethite is predominantly inherited from the Zn associated with the

ferrihydrite precursor. The exact mechanisms of Zn isotope fractionation during incorporation into goethite however, requires further investigations at varying pH and Zn/Fe molar ratios.

A Zn isotope fractionation of −1.18±0.15‰ is derived for Zn incorporation into Lep structure and is probably also caused by a complex suite of mineral nucleation and growth processes (Figure 3b). At the initial stage (< 1 min), finite Lep particles directly nucleate from solution,[56] and almost all the Zn is retained on the solids (Figure 3b). As the Lep crystals grow larger with time (1-60 min), part of the Zn is incorporated into the lattices, while part of the Zn is released back into solution, especially in the first 9 mins. The Zn released is probably that previously adsorbed on the solid surfaces during 0-1 min and is probably relatively heavy according to the adsorption experiments. This decreases the solid $\delta^{66/64}$Zn. After crystal growth is complete at ~1 h, Zn adsorption-desorption reactions dominate and probably approach equilibrium, and as-induced isotope exchanges occur simultaneously. During this stage, relatively heavy isotopes are adsorbed onto the Zn2Lep_n surfaces. This may consequently counteract the negative isotope fractionation during Zn incorporation into the lattices, resulting in the $\delta^{66/64}$Zn of Zn2Lep that is indistinguishable from that of the stock solution (Figure 4b, S8B).

The $\delta^{66/64}$Zn value for Zn2Fero is higher than the stock solution (Figure 4c, S8C), probably owing to the adsorption of heavy Zn isotopes onto the solids. Removal of the adsorbed Zn on the mineral surfaces by acid washing decreases the $\delta^{66/64}$Zn value of Zn2Fero_n so that it is indistinguishable from the stock solution. The negligible Zn isotope fractionation (0.06±0.11‰) in Zn2Fero_n is probably closely related to the fast crystal nucleation and growth that is almost complete in 1 min (Figure 3c). This is consistent with previous studies showing that the expression of kinetic isotope effects should be prevented in the solids when produced at extremely rapid precipitation rates.[28] Later (1-60 min), relatively heavy Zn isotopes in the residual solution pool are specifically adsorbed onto the solid surfaces, while at the same time, protons strongly compete for adsorption sites and drive the release of relatively light Zn isotopes into solution.[16]

568 The different $\Delta^{66/64}Zn_{substituted\text{-}stock\ solution}$ induced by Zn substitution for lattice Fe in
569 these FeOOH polymorphs may be strongly related to their different nucleation and
570 growth rates, in addition to their different formation pathways. Several previous studies
571 have examined the effects of precipitation rates on Fe isotope fractionation. In general,
572 typically small or almost no Fe isotope fractionation is observed when precipitation
573 occurs either very fast or very slowly (e.g., hundreds of days).[26, 30] Significant isotope
574 fractionations occur however, when the precipitation progresses over time scales of
575 hours to weeks.[26, 28] In the present study, the time scales for Zn2Goe_n and Zn2Lep_n
576 nucleation and growth range from 1 h to 12 h, while that for Zn2Fero_n is within 1 min
577 (Figure 3). The calculated $\Delta^{66/64}Zn_{substituted\text{-}stock\ solution}$ values for these Zn substituted
578 FeOOH polymorphs are also comparable to those for Fe(III) precipitated at similar
579 precipitation rates.[26, 30] As the initial crystal nucleation and growth rates for Zn2Goe_n
580 and Zn2Lep_n are relatively low, diffusion gradient-controlled Zn incorporation into
581 the growing solids results in the large negative isotope fractionations observed. But for
582 Zn2Fero_n, diffusion gradients in the liquid boundary layer around the primary
583 feroxyhyte nuclei may limit isotope exchange between the residual Zn in this layer and
584 the bulk aqueous pool and finally lead to no isotope fractionation upon the rapid Zn
585 retention by the solids.[26]

586 **4. Environmental Implications**

587 Various mineral-solution interfacial reactions, including adsorption and
588 substitution, contribute to a "black box" of isotope signals in both experimental and
589 environmental systems. In particular, adsorption and substitution with iron (hydr)oxides
590 play important roles in mediating element geochemical cycling, mobility and fate,
591 including the isotope fractionation factors of Zn in terrestrial environments. Here
592 preferential adsorption of heavy Zn isotopes onto FeOOH polymorph surfaces is
593 confirmed at circumneutral pH conditions. Moreover, the present study shows for the
594 first time that isotopically light Zn is incorporated into Fe (hydr)oxide structures. It is
595 recently reported that secondary minerals (e.g., Fe and Mn (hydr)oxides) during
596 pedogenesis enrich light Zn and Cu isotopes as internalized species, due to the
597 incorporation of these metals into Fe (hydr)oxides.[4, 13] Similarly, the enrichment of light

Zn isotopes in acid mine drainage precipitates, jarosite and goethite, relative to the drainage is also attributed to Zn incorporation into the solids.[8] Here we provide the first experimental evidence for these field observations. We observe larger fractionation factors ($\Delta^{66/64}Zn_{substituted\text{-}stock\ solution}$= -1.5‰ to -1.2‰) however, for Zn substituted goethite and lepidocrocite than the theoretical maximum of -0.7‰ for Zn incorporation into Fe (hydr)oxides based on available global soil data[4] and the range of –0.35‰ to –0.08‰ for Zn-substituted goethite[8]. This is probably caused by the different crystal nucleation and growth rates of these Zn-substituted Fe (hydr)oxides under experimental and field conditions[28] and highlights the important role that nucleation and growth processes play in Zn isotope fractionation with Fe (hydr)oxides. Further experimental studies conducted over a range of environmentally relevant conditions (e.g., circumneutral pH, micromolar concentrations of Zn and Fe, and low temperature) and with other minerals are necessary to constrain the theoretical range of Zn isotope fractionation during interactions with Fe (hydr)oxides, and further determine the most important processes responsible for Zn isotope fractionation in experimental and natural systems. As an additional implication of this work, the different Zn isotope fractionation directions observed between adsorption onto and incorporation into Fe (hydr)oxides might be used to identify the crystal chemistry of Zn in these minerals according to their Zn isotope compositions. Conclusively, these results reveal possible Zn isotope fractionation mechanisms during mineral-solution geochemical processes pertinent to Earth's critical zone and provide a mechanistic framework towards source tracing and process tracking Zn in contaminated and natural environments.

ASSOCIATED CONTENT

Supporting Information

Reagent information; details of Zn isotope ratio measurement; powder XRD, TEM, EDS and zeta potential analyses of obtained minerals; Zn macroscopic adsorption kinetics, adsorption edge, isotherms, and Zn isotope compositions in solid and aqueous phases and mass balance; isotope and chemical compositions of solutions and solids

obtained during the Zn substitution experiments; Rietveld structure refinement results of intermediates during Zn-doped FeOOHs formation; linear combination fitting analysis of Zn K-edge XANES spectra and structure parameters derived from Zn K-edge EXAFS fitting; Zn species calculation.

Notes

The authors declare no competing financial interest.

Acknowledgements

The authors gratefully thank the National Natural Science Foundations of China (Nos. 42077015, 41771267, 42277392 and 41977288), Key Science and Technology Projects of Inner Mongolia autonomous region (No. 2019ZD001), and the Fundamental Research Funds for the Central Universities (Grant 103-510320036) and Royal Society Newton Mobility Grant (IEC/NSFC/191423) for financial support.

REFERENCES

1. Jennings, A. A., Analysis of worldwide regulatory guidance values for the most commonly regulated elemental surface soil contamination. *J. Environ. Manage.* **2013,** *118*, 72-95.
2. Rout, G. R.; Das, P., Effect of metal toxicity on plant growth and metabolism: I. Zinc. In *Sustainable Agriculture*, Lichtfouse, E.; Navarrete, M.; Debaeke, P.; Véronique, S.; Alberola, C., Eds. Springer Netherlands: Dordrecht, 2009; pp 873-884.
3. Agency for Toxic Substances and Disease Registry (ATSDR). 2005. Toxicological profile for zinc. Atlanta, GA: U.S. Department of Health and Human Services, Public Health Service.
4. Little, S. H.; Munson, S.; Prytulak, J.; Coles, B. J.; Hammond, S. J.; Widdowson, M., Cu and Zn isotope fractionation during extreme chemical weathering. *Geochim. Cosmochim. Acta* **2019,** *263*, 85-107.
5. Liu, S. A.; Liu, P. P.; Lv, Y. W.; Wang, Z. Z.; Dai, J. G., Cu and Zn isotope fractionation during oceanic alteration: Implications for oceanic Cu and Zn cycles. *Geochim. Cosmochim. Acta* **2019,** *257*, 191-205.
6. Zhang, T.; Sun, R. Y.; Liu, Y.; Chen, L.; Zheng, W.; Liu, C. Q.; Chen, J. B., Copper and Zinc isotope signatures in scleratinian corals: Implications for Cu and Zn cycling in modern and ancient ocean. *Geochim. Cosmochim. Acta* **2022,** *317*, 395-408.
7. Ma, L.; Wang, W.; Xie, M. W.; Wang, W. X.; Evans, R. D., Using Zn isotopic signatures for source identification in a contaminated estuary of Southern China.

662 *Environ. Sci. Technol.* **2020,** *54*, (8), 5140-5149.
663 8. Liu, Y. H.; Gao, T.; Xia, Y. F.; Wang, Z. R.; Liu, C. S.; Li, S. H.; Wu, Q. Q.; Qi, M.;
664 Lv, Y. W., Using Zn isotopes to trace Zn sources and migration pathways in paddy soils
665 around mining area. *Environ. Pollut.* **2020,** *267*.
666 9. Wang, Z.; Kwon, K. D.; Peacock, C.; Mo, X.; Gou, W.; Feng, X.; Li, W., Zn stable
667 isotope fractionation during adsorption onto todorokite: A molecular perspective from
668 X-ray absorption spectroscopy and density functional theory. *Geochim. Cosmochim.*
669 *Acta* **2022,** *327*, 116-136.
670 10. Guinoiseau, D.; Gelabert, A.; Moureau, J.; Louvat, P.; Benedetti, M. F., Zn isotope
671 fractionation during sorption onto kaolinite. *Environ. Sci. Technol.* **2016,** *50*, (4), 1844-
672 52.
673 11. Mavromatis, V.; González, A. G.; Dietzel, M.; Schott, J., Zinc isotope fractionation
674 during the inorganic precipitation of calcite – Towards a new pH proxy. *Geochim.*
675 *Cosmochim. Acta* **2019,** *244*, 99-112.
676 12. Komárek, M.; Ratié, G.; Vaňková, Z.; Šípková, A.; Chrastný, V., Metal isotope
677 complexation with environmentally relevant surfaces: Opening the isotope
678 fractionation black box. *Crit. Rev. Environ. Sci. Technol.* **2022,** *52*, (20), 3573-3603.
679 13. Quantin, C.; Guinoiseau, D., The use of stable isotopes in soil science: Metals. In
680 *Reference Module in Earth Systems and Environmental Sciences*, Elsevier: 2022; pp 1-
681 8.
682 14. Fernandez, A.; Borrok, D. M., Fractionation of Cu, Fe, and Zn isotopes during the
683 oxidative weathering of sulfide-rich rocks. *Chem. Geol.* **2009,** *264*, (1-4), 1-12.
684 15. Opfergelt, S.; Cornelis, J. T.; Houben, D.; Givron, C.; Burton, K. W.; Mattielli, N.,
685 The influence of weathering and soil organic matter on Zn isotopes in soils. *Chem. Geol.*
686 **2017,** *466*, 140-148.
687 16. Weiss, D. J.; Boye, K.; Caldelas, C.; Fendorf, S., Zinc isotope fractionation during
688 early dissolution of biotite granite. *Soil Sci. Soc. Am. J* **2014**, (78), 171–179.
689 17. Yan, X. R.; Zhu, M. Q.; Li, W.; Peacock, C. L.; Ma, J. Y.; Wen, H. J.; Liu, F.; Zhou,
690 Z. B.; Zhu, C. W.; Yin, H., Cadmium isotope fractionation during adsorption and
691 substitution with iron (oxyhydr)oxides. *Environ. Sci. Technol.* **2021,** *55*, (17), 11601-
692 11611.
693 18. Pokrovsky, O. S.; Viers, J.; Freydier, R., Zinc stable isotope fractionation during its
694 adsorption on oxides and hydroxides. *J. Colloid Interf. Sci.* **2005,** *291*, (1), 192-200.
695 19. Juillot, F.; Maréchal, C.; Ponthieu, M.; Cacaly, S.; Morin, G.; Benedetti, M.;
696 Hazemann, J. L.; Proux, O.; Guyot, F., Zn isotopic fractionation caused by sorption on
697 goethite and 2-Lines ferrihydrite. *Geochim. Cosmochim. Acta* **2008,** *72*, (19), 4886-
698 4900.
699 20. Gou, W.; Li, W.; Ji, J.; Li, W., Zinc isotope fractionation during sorption onto Al
700 oxides: Atomic level understanding from EXAFS. *Environ. Sci. Technol.* **2018,** *52*, (16),
701 9087-9096.
702 21. Wasylenki, L. E.; Howe, H. D.; Spivak-Birndorf, L. J.; Bish, D. L., Ni isotope
703 fractionation during sorption to ferrihydrite: Implications for Ni in banded iron
704 formations. *Chem. Geol.* **2015,** *400*, 56-64.
705 22. Wasylenki, L. E.; Swihart, J. W.; Romaniello, S. J., Cadmium isotope fractionation

during adsorption to Mn oxyhydroxide at low and high ionic strength. *Geochim. Cosmochim. Acta* **2014,** *140*, 212-226.
23. Weiss, D.; Northover, G.; Hanif, M.; García-España, E.; Vilar, R.; Arnold, T.; Markovic, T.; Wissuwa, M.; Delgado, E., Isotope fractionation of zinc in the paddy rice soil-water environment and the role of 2'deoxymugineic acid (DMA) as zincophore under Zn limiting conditions. *Chem. Geol.* **2021,** *577*.
24. Aucour, A.-M.; Bedell, J.-P.; Queyron, M.; Tholé, R.; Lamboux, A.; Sarret, G., Zn speciation and stable isotope fractionation in a contaminated urban wetland soil–Typha latifolia system. *Environ. Sci. Technol.* **2017,** *51*, (15), 8350-8358.
25. Nelson, J.; Wasylenki, L.; Bargar, J. R.; Brown, G. E.; Maher, K., Effects of surface structural disorder and surface coverage on isotopic fractionation during Zn(II) adsorption onto quartz and amorphous silica surfaces. *Geochim. Cosmochim. Acta* **2017,** *215*, 354-376.
26. Skulan, J. L.; Beard, B. L.; Johnson, C. M., Kinetic and equilibrium Fe isotope fractionation between aqueous Fe(III) and hematite. *Geochim. Cosmochim. Acta* **2002,** *66*, (17), 2995-3015.
27. Clayton, R. E.; Hudson-Edwards, K. A.; Malinovsky, D.; Andersson, P., Fe isotope fractionation during the precipitation of ferrihydrite and transformation of ferrihydrite to goethite. *Mineral. Mag.* **2005,** *69*, (5), 667-676.
28. Balci, N.; Bullen, T. D.; Witte-Lien, K.; Shanks, W. C.; Motelica, M.; Mandernack, K. W., Iron isotope fractionation during microbially stimulated Fe(II) oxidation and Fe(III) precipitation. *Geochim. Cosmochim. Acta* **2006,** *70*, (3), 622-639.
29. Guinoiseau, D.; Galer, S. J. G.; Abouchami, W., Effect of cadmium sulphide precipitation on the partitioning of Cd isotopes: Implications for the oceanic Cd cycle. *Earth and Planet. Sci. Lett.* **2018,** *498*, 300-308.
30. Johnson, C. M.; Skulan, J. L.; Beard, B. L.; Sun, H.; Nealson, K. H.; Braterman, P. S., Isotopic fractionation between Fe(III) and Fe(II) in aqueous solutions. *Earth Planet. Sci. Lett.* **2002,** *195*, (1), 141-153.
31. Hu, B.; Yan, X.; Wang, W.; Li, Y.; Li, H.; Hong, M.; Liu, F.; Yin, H., Iron oxyhydroxide polytype (γ-, δ- and β-FeOOH) structures govern Zn mobility. *Chem. Geol.* **2022**, 121167.
32. Manceau, A.; Nagy, K. L.; Spadini, L.; Ragnarsdottir, K. V., Influence of anionic layer structure of Fe-oxyhydroxides on the structure of Cd surface complexes. *J. Colloid Interface Sci.* **2000,** *228*, (2), 306-316.
33. Liu, L.; Wang, X. M.; Zhu, M. Q.; Ma, J. Y.; Zhang, J.; Tan, W. F.; Feng, X. H.; Yin, H.; Liu, F., The speciation of Cd in Cd–Fe coprecipitates: Does Cd substitute for Fe in goethite structure? *ACS Earth Space Chem.* **2019,** *3*, (10), 2225-2236.
34. Gou, W.; Li, W.; Siebecker, M. G.; Zhu, M.; Li, L.; Sparks, D. L., Coupling molecular-scale spectroscopy with stable isotope analyses to investigate the effect of Si on the mechanisms of Zn–Al LDH formation on Al oxide. *Environ. Sci. Technol.* **2022,** *56*, (19), 13829-13836.
35. Zhu, C.; Liao, S.; Wang, W.; Zhang, Y.; Yang, T.; Fan, H.; Wen, H., Variations in Zn and S isotope chemistry of sedimentary sphalerite, Wusihe Zn-Pb deposit, Sichuan Province, China. *Ore Geol. Rev.* **2018,** *95*, 639-648.

750 36. Pallavicini, N.; Engström, E.; Baxter, D. C.; Öhlander, B.; Ingri, J.; Rodushkin, I.,
751 Cadmium isotope ratio measurements in environmental matrices by MC-ICP-MS. *J.*
752 *Anal. At. Spectrom.* **2014,** *29*, (9), 1570-1584.
753 37. Archer, C.; Andersen, M. B.; Cloquet, C.; Conway, T. M.; Dong, S.; Ellwood, M.;
754 Moore, R.; Nelson, J.; Rehkämper, M.; Rouxel, O.; Samanta, M.; Shin, K.; Sohrin, Y.;
755 Takano, S.; Wasylenki, L., Inter-calibration of a proposed new primary reference
756 standard AA-ETH Zn for zinc isotopic analysis. *J. Anal. Atom. Spectrom.* **2017,** *32*, (2),
757 415-419.
758 38. Wang, Z.-Z.; Liu, S.-A.; Liu, J.; Huang, J.; Xiao, Y.; Chu, Z.-Y.; Zhao, X.-M.; Tang,
759 L., Zinc isotope fractionation during mantle melting and constraints on the Zn isotope
760 composition of Earth's upper mantle. *Geochim. Cosmochim. Acta* **2017,** *198*, 151-167.
761 39. Ravel, B.; Newville, M., ATHENA, ARTEMIS, HEPHAESTUS: data analysis for
762 X-ray absorption spectroscopy using IFEFFIT. *J. Synchrotron Radiat.* **2005,** *12*, 537-
763 541.
764 40. Kelly, S. D.; Hesterberg, D.; Ravel, B., Analysis of Soils and Minerals Using X-
765 ray Absorption Spectroscopy. In *Methods of Soil Analysis Part 5—Mineralogical*
766 *Methods*, Soil Science Society of America: 2008; pp 387-463.
767 41. Schauble, E. A., Applying stable isotope fractionation theory to new systems. *Rev.*
768 *Mineral. Geochem.* **2004,** *55*, (1), 65-111.
769 42. Waychunas, G. A.; Fuller, C. C.; Davis, J. A.; Rehr, J. J., Surface complexation and
770 precipitate geometry for aqueous Zn(II) sorption on ferrihydrite: II. XANES analysis
771 and simulation. *Geochim. Cosmochim. Acta* **2003,** *67*, (5), 1031-1043.
772 43. Cismasu, A. C.; Levard, C.; Michel, F. M.; Brown, G. E., Properties of impurity-
773 bearing ferrihydrite II: Insights into the surface structure and composition of pure, Al-
774 and Si-bearing ferrihydrite from Zn(II) sorption experiments and Zn K-edge X-ray
775 absorption spectroscopy. *Geochim. Cosmochim. Acta* **2013,** *119*, 46-60.
776 44. Aucour, A.; Bedell, J.; Queyron, M.; Magnin, V.; Testemale, D.; Sarret, G.,
777 Dynamics of Zn in an urban wetland soil–plant system: Coupling isotopic and EXAFS
778 approaches. *Geochim. Cosmochim. Acta* **2015,** *160*, 55-69.
779 45. Frierdich, A. J.; Catalano, J. G., Controls on Fe(II)-activated trace element release
780 from goethite and hematite. *Environ Sci. Technol.* **2012,** *46*, (3), 1519-1526.
781 46. Frierdich, A. J.; Scherer, M. M.; Bachman, J. E.; Engelhard, M. H.; Rapponotti, B.
782 W.; Catalano, J. G., Inhibition of trace element release during Fe(II)-activated
783 recrystallization of Al-, Cr-, and Sn-substituted goethite and hematite. *Environ. Sci.*
784 *Technol.* **2012,** *46*, (18), 10031-10039.
785 47. Trivedi, P.; Axe, L.; Tyson, T. A., An analysis of zinc sorption to amorphous versus
786 crystalline iron oxides using XAS. *J. Colloid Interface Sci.* **2001,** *244*, (2), 230-238.
787 48. Roberts, D. R.; Ford, R. G.; Sparks, D. L., Kinetics and mechanisms of Zn
788 complexation on metal oxides using EXAFS spectroscopy. *J. Colloid Interf. Sci.* **2003,**
789 *263*, (2), 364-376.
790 49. Waychunas, G. A.; Fuller, C. C.; Davis, J. A., Surface complexation and precipitate
791 geometry for aqueous Zn(II) sorption on ferrihydrite I: X-ray absorption extended fine
792 structure spectroscopy analysis. *Geochim. Cosmochim. Acta* **2002,** *66*, (7), 1119-1137.
793 50. Bochatay, L.; Persson, P., Metal ion coordination at the water–manganite (γ-

MnOOH) interface: II. An EXAFS study of zinc(II). *J. Colloid Interf. Sci.* **2000,** *229*, (2), 593-599.
51. Kaur, N.; Gräfe, M.; Singh, B.; Kennedy, B., Simultaneous incorporation of Cr, Zn, Cd, and Pb in the goethite structure. *Clays Clay Miner.* **2009,** *57*, (2), 234-250.
52. Bryan, A. L.; Dong, S.; Wilkes, E. B.; Wasylenki, L. E., Zinc isotope fractionation during adsorption onto Mn oxyhydroxide at low and high ionic strength. *Geochim. Cosmochim. Acta* **2015,** *157*, 182-197.
53. Balistrieri, L. S.; Borrok, D. M.; Wanty, R. B.; Ridley, W. I., Fractionation of Cu and Zn isotopes during adsorption onto amorphous Fe(III) oxyhydroxide: Experimental mixing of acid rock drainage and ambient river water. *Geochim. Cosmochim. Acta* **2008,** *72*, (2), 311-328.
54. Fujii, T.; Moynier, F.; Blichert-Toft, J.; Albarède, F., Density functional theory estimation of isotope fractionation of Fe, Ni, Cu, and Zn among species relevant to geochemical and biological environments. *Geochim. Cosmochim. Acta* **2014,** *140*, 553-576.
55. Liu, J.; Sheng, A.; Li, X.; Arai, Y.; Ding, Y.; Nie, M.; Yan, M.; Rosso, K. M., Understanding the importance of labile Fe(III) during Fe(II)-catalyzed transformation of metastable iron oxyhydroxides. *Environ. Sci. Technol.* **2022,** *56*, (6), 3801-3811.
56. Cornell, R. M.; Schwertmann, U., Formation. In *The iron oxides: structure, properties, reactions, occurrences, and uses*, Second ed.; John Wiley & Sons: 2003; pp 345-364.